Converting waste PET plastics into automobile fuel and antifreeze components

Chen Zhao (czhao@chem.ecnu.edu.cn)
East China Normal University
Zhiwen Gao
East China Normal University
Shuang Chen
East China Normal University
Bing Ma
East China Normal University
Jingqing Tian
East China Normal University

Article

Keywords: plastic pollution, polyethylene terephthalate, sustainability

Posted Date: October 21st, 2021

DOI: https://doi.org/10.21203/rs.3.rs-969098/v1

Version of Record: A version of this preprint was published at Nature Communications on June 10th, 2022. See the published version at https://doi.org/10.1038/s41467-022-31078-w.

Abstract

With the aim to solve the serious problem of white plastic pollution, we report herein a H_2-free low-cost Cu/SiO_2 catalyzed process to convert polyethylene terephthalate (PET) into *p*-xylene (PX) and ethylene glycol (EG) in one pot with methanol as both the solvent and hydrogen source at 210 °C. Kinetic and *in-situ* Fourier-transform infrared spectroscopy (FTIR) studies demonstrated that the degradation of PET into dimethyl terephthalate (DMT) in methanol involved methanol dehydrogenation and ester hydrodeoxygenation reactions. When preparing the copper silicate precursor using the hydrothermal method with ammonia, NaCl was introduced to interact with the surface hydroxyl groups of SiO_2, thereby forming a dense, granular copper silicate with a high Cu^+/Cu^0 ratio, which improved the methanol dehydrogenation and DMT hydrodeoxygenation activities. This novel H_2-free process uses a low-cost Cu-based catalyst, allowing us to produce gasoline and antifreeze components from waste PET plastic in one pot, which provides a feasible solution to the plastic pollution problem in islands.

Introduction

Polyethylene terephthalate (PET) is the most abundant polyester plastic with nearly 70 million tons produced per year worldwide[1]. However, PET is not easily degradable after use[2, 3]. Ten million tons of PET waste are discharged into the ocean annually, and the amount of PET residues from the textile and packaging industries is especially high[4, 5]. As a result, the health of marine organisms is being seriously threatened[6, 7]. Depolymerization and reuse of PET are the most common methods to solve this problem. Current chemical depolymerization methods include hydrolysis, alcoholysis, and ammonolysis[8-11]. However, these methods still face limitations including harsh reaction conditions, low product yield, and separation difficulties.

Recent trends in solving marine plastic pollution have led to a proliferation of studies on PET chemical processing. Jing et al.[12] used Ru/Nb_2O_5 to convert aromatic plastics such as PET, polystyrene (PS), polycarbonate (PC), and polyphenylene ether (PPE), fabricated from aromatic monomers by interunit C–O and/or C–C linkages, to various chemicals such as arenes (75–85% yield). Lu et al.[13] used the ethylene glycol fragments in the PET structure to provide a hydrogen source for the conversion of PET into benzene, toluene, and *p*-xylene (BTX) over a Ru/Nb_2O_5 catalyst and obtained a 72.7–93.3% BTX yield. However, the use of Ru as the metal active center increased the cost of the catalyst, resulting in a complex mixture of products. Similarly, Yan et al.[14] demonstrated the conversion of PET into arenes *via* depolymerization and hydrodeoxygenation over a Co/TiO_2 catalyst with 75.2 mol% *p*-xylene and toluene selectivity under 30 bar initial H_2 pressure at 340 °C. Tang et al.[15] selectively synthesized gasoline and jet fuel range C_7–C_8 cycloalkanes and aromatics by a three-step reaction. Dimethyl terephthalate (DMT) was first obtained from the alcoholysis of PET and was subsequently solvent-free hydrogenated to cyclohexane-1,4-dicarboxylate (DMCD) on Pt/C. Finally, DMCD was hydrodeoxygenated to gasoline and jet fuel range cyclic hydrocarbons on a bimetallic $Ru\text{-}Cu/SiO_2$ catalyst. Lately, photocatalytic and electrocatalytic reforming for PET waste upcycling became a novel strategy. Erwin et al.[16] reported the efficient photoreforming of PET into H_2 fuel and organic products such as formate, acetate and pyruvate under ambient temperature and pressure. Duan et al.[17] reported electrocatalytic upcycling of PET to potassium diformate and terephthalic acid and H_2 fuel. The electrocatalyst ($CoNi_{0.25}P$) is developed to achieve a current density of 500 mA cm^{-2} at 1.8 V in a membrane-electrode assembly reactor with > 80 % of faradaic efficiency and selectivity to formate.

Chemical processing of other plastics is also being studied widely. Scott et al.[18] proposed a new method for converting waste polyethylene into higher-value long-chain alkyl aromatics at low temperatures. This method combined two chemical reactions: hydrogenolysis and aromatization. The process used a $Pt/\gamma\text{-}Al_2O_3$ catalyst to directly convert low-density polyethylene into long-chain alkyl aromatic hydrocarbons and alkyl naphthenates with an average carbon number of about 30 at 280 °C. The yield reached ca. 80% after 24 h. Tennakoon et al.[19] cut large molecules into precise atomic-sized fragments using enzymes and subsequently designed $m SiO_2/Pt/SiO_2$ catalysts with an ordered mesoporous shell/active-site/core structure. The distribution of alkane products could be adjusted by modulating the sizes of the mesoporous pores of the catalysts.

In this study, we developed a H_2-free one-pot method to directly convert PET wastes into *p*-xylene (PX) and ethylene glycol (EG) using a low-cost Cu-based catalyst (Figure 1). Through this process, PET was directly degraded to DMT in methanol without a special catalyst. Methanol served as a source of hydrogen for subsequent hydrogenation reactions by dehydrogenation. The structure and formation

process of Cu/SiO_2 upon addition of NaCl were characterized in detail, and the reaction mechanism for PET conversion was studied through kinetic and *in-situ* Fourier-transform infrared spectroscopy (FTIR) studies simultaneously.

Results And Discussion

The integrated system allowing PET depolymerization and conversion coupled three reaction steps: PET methanolysis, methanol dehydrogenation, and DMT hydrodeoxygenation. Experiments demonstrated that the alcoholysis of PET could be directly carried out in methanol at 210°C in the absence of the catalyst to obtain a 100% yield of DMT monomers within 30 min (Figure S1). Therefore, we mainly focused on catalysts for methanol dehydrogenation and DMT hydrodeoxygenation. Table 1 lists the performances of different catalysts in these processes. Almost all the catalysts tested were inactive, except Cu/SiO_2 (HT) with a 73% yield of PX, while the yield of the by-product methyl 4-methylbenzoate and 4-methylbenzyl alcohol were 23% and 4%, respectively. Interestingly, Co/SiO_2, Ni/SiO_2, and Fe/SiO_2 showed no activity for the whole reaction. Once PET was depolymerized into DMT monomers, the hydrodeoxygenation reaction stopped since Co, Ni, and Fe active centers hardly catalyzed methanol dehydrogenation, resulting in a lack of hydrogen for DMT hydrodeoxygenation.

Table 1
Catalytic performance of different catalysts used in the PET conversion process.

Catalyst	PET Conv. (%)	EG/DMT yield (%)	DMT Conv. (%)	PX yield (%)	By-product yield (%)		Incremental pressure at RT (MPa)	Gas composition (MPa)			
					Methyl 4-methylbenzoate	4-methylbenzyl alcohol		H_2	CO	CO_2	CH_4
Cu/SiO_2(HT)	100	100	100	73	23	4.0	2.9	73	24	3	
Co/SiO_2	100	100	-	-	-	-	-	-	-	-	-
Ni/SiO_2	100	100	-	-	-	-	-	-	-	-	-
Fe/SiO_2	100	100	-	-	-	-	-	-	-	-	-
Cu/TiO_2	100	100	100	17	57	27	1.2	69	28	2	1
Cu/ZrO_2	100	100	-	-	-	-	-	-	-	-	-
Cu/CeO_2	100	100	-	-	-	-	-	-	-	-	-
Cu/SiO_2(IM)	100	100	-	-	-	-	-	-	-	-	-
Cu/SiO_2(DPU)	100	100	-	-	-	-	-	-	-	-	-
Cu/SiO_2(DPA)	100	100	2.2	-	2.2	-	0.8	53	35	12	-
$CuNa/SiO_2$	100	100	100	100	-	-	3.4	75	21	4	-
$CuLi/SiO_2$	100	100	100	89	8.4	2.2	3.0	79	18	3	-
CuK/SiO_2	100	100	100	97	1.9	0.7	3.3	73	23	4	-
$CuRb/SiO_2$	100	100	100	60	18	22	3.0	74	23	3	-
$CuCs/SiO_2$	100	100	100	67	20	13	3.0	73	22	5	-

Reaction conditions: 0.12 g PET, 0.1 g catalyst, 30 mL methanol, 210°C, 6 h.

HT: Hydrothermal method, IM: Impregnation method, DPA: Deposition–precipitation with ammonia method, DPU: Deposition–precipitation with urea method, RT: Room temperature, EG: Ethylene glycol, DMT: Dimethyl terephthalate, and PX: *p*-xylene.

Table of content

We subsequently used Cu as the metal active center to investigate the influence of the support on this reaction. Unlike Cu/SiO_2, Cu/TiO_2 (PX yield 17%), Cu/CeO_2 and Cu/ZrO_2 (PX yield 0%) did not show good performances. We speculated that SiO_2 had a more amorphous structure than TiO_2, CeO_2, and ZrO_2 and was easily etched by ammonia to form a strong copper silicate structure. This copper silicate precursor structure was beneficial to partially reduce Cu^+ and Cu^0 for methanol dehydrogenation. The synthesis methods of Cu/SiO_2 were investigated by comparing the effects of various Cu-based catalysts on the conversion of PET. Several Cu-based catalysts were prepared using various methods such as the hydrothermal method (HT), impregnation method (IM), deposition–precipitation with urea (DPU), and deposition–precipitation with ammonia (DPA). Only the Cu/SiO_2 catalysts prepared by HT and DPA showed reactivity towards methanol dehydrogenation, producing hydrogen at 2.9 and 0.8 MPa, respectively. As indicated above, this hydrogen can be used for subsequent DMT hydrodeoxygenation. However, hydrodeoxygenation of PET on Cu/SiO_2 (DPA) stopped at intermediate methyl 4-methylbenzoate, most likely because of the lack of H_2 released during the methanol dehydrogenation to completely convert PET to PX. Unlike the HT and DPA methods, the Cu species of the catalyst prepared by the IM and DPU methods generated Cu^0 species after being completely reduced (Figure S2). In previous work[20−22], it was proven that a mixture of Cu_2O and Cu was the active site for methanol dehydrogenation. This could explain the low activity of Cu/SiO_2 (IM) and Cu/SiO_2 (DPU) to provide the required H_2 for DMT hydrodeoxygenation reactions. Finally, we attempted to introduce alkali metals (e.g., Na, Li, K, Rb, and Cs) in the form of chlorides via a hydrothermal treatment to investigate the catalyst activity. A 100% PX yield was obtained on $CuNa/SiO_2$ (HT) (Figure S3). Thus, the addition of NaCl significantly promoted the conversion of PET to PX on Cu/SiO_2 (HT). We tried to use $CuNa/SiO_2$ for cyclic reaction tests (Table S1). The used catalyst can still maintain a PX yield of 96% in the second bath, but when the third bath is performed, the PX yield is reduced to 52.7%. The main reason is that the Cu species is converted to Cu^0 in a hydrogen atmosphere. The active sites of the hydrogenation reaction are reduced as a result.

To study the influence of NaCl on the hydrothermal treatment, a series of characterization methods were used on the catalyst with and without the addition of NaCl. Cu/SiO_2 (dried) and $CuNa/SiO_2$ (dried) samples prepared by the HT method exhibited X-ray diffraction (XRD) peaks characteristics of $Cu_2Si_2O_5(OH)_2$ (2θ = 19.9, 21.8, 30.8, 35.0, 57.5, and 62.4° (PDF #27-0188)) (Figure 2a). The addition of NaCl reduced the crystallinity of copper silicate and the size of Cu nanoparticles, resulting in more uniform size distribution. The peaks for copper silicate disappeared after air-calcination and reduction, and they were replaced by Cu characteristics peaks (2θ = 43.3° (PDF #04-0836)) and Cu_2O (2θ = 36.4, 42.3, 61.3, and 77.3° (PDF #05-0667)) (Figure S4). The N_2 adsorption–desorption showed that the specific surface area and mesoporous volume of the Cu/SiO_2 (dried) precursor were 277.9 m^2/g and 0.08 cm^3/g, respectively (Figure 2b). After the addition of Na^+, the specific surface area decreased by 5/6 (46.9 m^2/g), and the mesoporous volume also decreased significantly (0.06 cm^3/g). Overall, the entire structure became denser.

The hydrogen temperature-programmed reduction (H_2-TPR) profile of the dried Cu/SiO_2 precursor sample showed reduction peaks at 256 and 280°C (Figure S5a), ascribed to the reduction of copper silicate to Cu^+ and Cu^0, respectively. After the addition of NaCl, reduction peaks appeared at higher temperatures of 274 and 299°C, revealing a stronger interaction between Cu particles and the support. The CO adsorption FTIR spectra of the reduced Cu/SiO_2 and $CuNa/SiO_2$ showed absorption vibration peaks of CO probe molecules at 2117 and 2111 cm^{-1}, respectively. Moreover, Cu/SiO_2 contained Cu^0 (band at 2133 cm^{-1}) species, while $CuNa/SiO_2$ showed the presence of Cu^+ (band at 2124 cm^{-1}) (Figure S5b). We measured the FTIR spectra of different states of Cu/SiO_2 and $CuNa/SiO_2$ (Figures S5c–e) and found that both dried samples showed a characteristic O-H stretching vibration peak at 669 cm^{-1}, which was ascribed to the copper silicate species, in line with the XRD results. The peak at 795 cm^{-1} was attributed to the bending vibrations of the Si-O bond of the amorphous silica support. The relative content of copper silicate was determined by the intensities of two peaks (i.e., I_{667}/I_{795}). After air-calcination, the intensity of the characteristic peak of copper silicate decreased slightly, while the peak of the carrier increased. This may be explained in terms of a lower crystallinity since copper silicate lost part of the crystal water during the calcination process. Moreover, the characteristic peak at 669 cm^{-1} nearly disappeared in the reduced sample, revealing that copper silicate may have been reduced to other Cu species by hydrogen. The thermogravimetric analysis (TGA) profile of the precursor (Figure S6) showed that physisorbed water from the precursor was removed at a temperature lower than 130°C. As the temperature increased to 600°C, crystal water was gradually removed, and the copper silicate decomposed into CuO and SiO_2. After the addition of NaCl, the water content of the precursor decreased (9.16%), and its structure was more compact. The significant weight loss at 1000–1145°C corresponded to the decomposition of CuO into Cu_2O.

Cu X-ray photoelectron spectroscopy (XPS) and Auger Cu LMM analysis were performed to elucidate the chemical states of Cu. Cu^{2+} satellite peaks at 920–950 eV revealed an incomplete reduction of the precursor (Figures 2d and f). The characteristic peaks for Cu_2O and Cu (952.2 and 932.1 eV) were too close to be distinguished by XPS. We intuitively determined the Cu^+/Cu^0 ratio by Cu LMM X-ray induced Auger electron spectroscopy (XAES, Figure 2c and e). The higher Cu^+/Cu^0 ratio (1.86) of $CuNa/SiO_2$ confirmed that after the addition of Na^+, copper silicate with a low crystallinity and a dense texture was less likely to be reduced to Cu^0. A higher ratio of Cu^+/Cu^0 was indicative of a higher tendency to both methanol dehydrogenation and DMT hydrodeoxygenation.

Transmission electron microscopy (TEM) images intuitively showed the different morphologies of the two copper silicates formed with and without NaCl introduction during the hydrothermal process. Thus, while the dried precursor of Cu/SiO_2 showed a layered copper silicate structure (Figure 2g), the dried precursor of $CuNa/SiO_2$ showed a special state of granular particle accumulation (Figure 2i). After reduction under H_2, high-resolution transmission electron microscopy (HRTEM) revealed a Cu particle size distribution in $CuNa/SiO_2$ centered at 3.9 ± 0.9 nm (Figure 2j), while Cu/SiO_2 showed smaller Cu particle sizes (5.1 ± 1.5 nm) (Figure 2h). TEM-mapping confirmed that Cu and Na were uniformly distributed on SiO_2 (Figures 2o and l).

Based on the characterization results, we propose a mechanism to explain the effect of NaCl addition on the formation mechanism of Cu/SiO_2 during the hydrothermal process. In the traditional hydrothermal synthesis process, layered copper silicate is normally formed, with Cu/Cu_2O particles being located on the layered structure after calcination and reduction. With the addition of NaCl, a large amount of Na^+ occupied the hydroxyl group sites on the SiO_2 surface, inhibiting nucleation of layered copper silicate and normally grown of this phase into a complete crystal shape. Thus, copper silicate finally exhibited a state of granular particle accumulation. Compared with traditional Cu/SiO_2, the granular copper silicate with poor crystallinity formed after the addition of Na^+ had a very dense structure, with a specific surface area of 46.9 m^2/g and a mesopore volume of 0.06 cm^3/g. H_2-TPR revealed that this dense structure was relatively difficult to reduce (Figure S5a), thus resulting in a higher number of active sites (i.e., high Cu^+/Cu^0 ratio of 1.86). SEM (Figure S7) showed that Cu^+/Cu^0 particles of $CuNa/SiO_2$ were smaller and more uniformly distributed after air calcination and hydrogen reduction.

We investigated the influence of the different Na^+/Cu^{2+} molar ratios generated during the hydrothermal treatment on the performance of $CuNa/SiO_2$. Thus, Na^+/Cu^{2+} molar ratios of 2.5:1, 5:1, 10:1, and 15:1 were denoted as 2.5 NaCl, 5 NaCl, 10 NaCl, and 15 NaCl, respectively. Based on the conversion tests of PET at 210°C, the yield of PX exhibited a volcano-type distribution (Figure S8a), with a maximum PX yield of 100% reached for the 5 NaCl sample, while samples 2.5 NaCl, 10 NaCl, and 15 NaCl showed lower yields of 78.3, 92.3, and 60.7%, respectively. To further explore the influence of the addition of NaCl on the formation of the catalyst, we carried out a series of characterization tests. The precursor samples all showed the characteristic diffraction peaks of the $Cu_2Si_2O_5(OH)_2$ crystal phase (Figure S9), indicating that the addition of NaCl did not affect the phase composition of the catalyst. In the case of the 5 NaCl sample, the copper silicate had poor crystallinity compared to other samples. TGA tests of the $CuNa/SiO_2$ precursor showed that physisorbed water (2.41%) and crystal water (6.75%) upon addition of 5 NaCl was the lowest among all the samples tested (Figures S10 and S8b). This also confirmed that the copper silicate structure was denser at this ratio, facilitating the removal of water during the calcination process. N_2 adsorption–desorption (Figure S11) revealed $CuNa/SiO_2$ to have the lowest surface area (46.9 m^2/g) upon addition of 5 NaCl (Figure S8c), indicating that the formed structure was the most compact among the samples tested herein. In the Cu LMM XAES spectra of the $CuNa/SiO_2$ after reduction, the ratio of Cu^+/Cu^0 still presented a volcano-type distribution (Figure S8d), and the Cu^+/Cu^0 ratio of $CuNa/SiO_2$ was the highest when 5 NaCl was introduced (1.86, Figure S12).

Based on the above observations, we speculated that, in the traditional hydrothermal synthesis process, Cu^{2+} in the solution combined with the silanol groups on the SiO_2 surface to form copper silicate, which accelerated the layered copper silicate nucleation and growth significantly. This type of layered copper silicate showed a low interface area with SiO_2, leading to a low Cu^+/Cu^0 ratio on the layered copper silicate surface (Figure 3a). A large amount of Na^+ occupied the silanol on the surface of the SiO_2 upon addition of 5 NaCl, thereby inhibiting nucleation and growth of layered copper silicate. Cu^{2+} in the solution could only be combined with the remaining silanol on the SiO_2 surface to form scattered and isolated copper silicate particles, and the compact structure had a small surface area and poor crystallinity. The formed granular copper silicate showed a large interface area with SiO_2. Granular copper silicate was more difficult to reduce compared with traditional layered copper silicate, resulting in a high ratio of Cu^+/Cu^0 active sites in the prepared catalyst (Figure 3b). However, when the amount of added NaCl was too high, Na^+ occupied all the silanol sites on SiO_2, resulting in the

precipitation of Cu^{2+} with SiO_3^{2-} in solution to form copper silicate, which was then deposited on the SiO_2 surface. Compared to the catalyst with 5 NaCl introduced during hydrothermal treatment, this type of copper silicate showed better crystallinity (Figure S7a) and was relatively easier to reduce to $Cu/Cu_2O{\cdot}SiO_2$ with a low ratio of Cu^+/Cu^0 (Figure 3c). In general, the addition of NaCl in the hydrothermal treatment resulted in the formation of granular copper silicate with a lower crystallinity, smaller specific surface area, and denser texture. When NaCl was introduced, Cu^+/Cu^0 showed a volcano-type curve distribution. When the molar mass ratio of Na^+/Cu^{2+} reached 5:1, the Cu^+/Cu^0 ratio reached the maximum (1.86), providing significantly more active sites for methanol dehydrogenation and DMT hydrodeoxygenation.

Finally, to ascertain whether the addition of NaCl only affected the formation process of copper silicate or could promote the reaction itself, we prepared a Cu/SiO_2-HT-Na-IM sample. We first synthesized Cu/SiO_2 by a hydrothermal method, which was subsequently impregnated with NaCl after the formation of layered copper silicate. The new copper silicate precursor has the same loading of Na^+ (2.4%) (Table S2) as $CuNa/SiO_2$. XRD (Figure S13) showed that the impregnated Na^+ did not affect the formation of copper silicate, although the yield of PX was moderate (65.8%). Thus, we confirmed that the addition of NaCl in the hydrothermal treatment affected the morphology of the copper silicate and therefore the Cu^+/Cu^0 ratio after reduction. Na impregnation after the formation of copper silicate not only failed to promote the catalyst activity but also inhibited some of the active sites by covering them, resulting in a reduction in the yield of PX.

We used $CuNa/SiO_2$ to conduct a kinetics study on the reaction of DMT (A) and the intermediates at the optimal reaction temperature (210°C) and monitored the distribution of products over time. As soon as the reaction started, the DMT concentration decreased (Figure 4a) at an initial rate of 0.36 g/g/h, revealing a high efficiency for hydrogen production. Hydrogen was produced during the heating process, and it was sufficient to maintain the amount of hydrogen required for the next reaction. When the reaction started, the intermediate methyl 4-methylbenzoate (C) was produced and a maximum yield of 24.3% at 1.5 h. Within 1–1.5 h, the intermediate 4-methylbenzyl alcohol (D) was produced slowly. At 3 h, almost all the DMT was converted, while the yield of the target product PX reached 100% at 6 h.

In this kinetics study, we only observed two intermediates: C and D. Importantly, we did not observe 1,4-benzenedimethanol, which implied that DMT underwent one-sided adsorption on $CuNa/SiO_2$. Therefore, methyl 4-(methylol)benzoate (B) may appear transitorily as an intermediate product. Based on these results, we speculated that the reaction from DMT to PX involved four steps: (1) one-sided adsorption of the ester of DMT on $CuNa/SiO_2$ and subsequent hydrogenation to alcohol, yielding B; (2) alcohol of B underwent hydrogenolysis to methyl groups and desorbed to form C; (3) ester C adsorbed on $CuNa/SiO_2$ and was hydrogenated to alcohol and obtain D; (4) alcohol D underwent hydrogenolysis to methyl groups and desorbed to obtain the target product PX. The kinetics of the three intermediates were studied under the same conditions (Figures 4b, 4c and 4d). Intermediates A, B, C, and D were completely consumed after approximately 5, 1.5, 5, and 1 h, respectively. The experimental results confirmed our proposed reaction pathway. The simulation results performed using MATLAB yielded the rate constants of each step (k_1 = 0.0138 min^{-1}, k_2 = 0.0424 min^{-1}, k_3 = 0.0103 min^{-1}, k_4 = 0.0632 min^{-1}). It is worth noting that C was obtained with the largest concentration after the DMT hydrogenation. This was because steps (2) and (3) required intermediate C desorption and re-adsorption on $CuNa/SiO_2$, making the hydrogenation of C the rate-determining step (k_3 = 0.0103 min^{-1}) of the overall process. The rate of alcohol hydrogenolysis was about 4–6 times that of the ester hydrogenation.

In-situ FTIR also demonstrated our reaction process of DMT and its intermediates (B, C, and D) on $CuNa/SiO_2$. The different substrate functional groups appeared in four regions in the FTIR spectra: (1) aryl C=C, 1494, 1523 cm^{-1}, (2) aryl C=O, 1594–1664 cm^{-1}, (3) aryl -CH_3 stretching, 2950–2863 cm^{-1}, and (4) O-H, 3305–3290 cm^{-1}. It should be noted that the aryl C=C band of the four substrates at 1494 and 1523 cm^{-1} did not change during the reaction (Figures 4e, 4f, 4g, and 4h), revealing that the aromatic structure remained intact during the process, and aromatic hydrocarbons tended to be generated. The intensity of the C=O stretching vibration peak at 1594–1664 cm^{-1} for intermediates A, B, and C decreased continuously with time until complete vanishment (Figures 4e, 4f, and 4g). This phenomenon indicated that the hydrogenation reaction occurred continuously under *in-situ* conditions. A and C, which lacking hydroxyl groups itself, produced O-H vibration peaks at 3305–3290 cm^{-1} and then gradually disappeared (Figures 4e and 4g), indicating that C=O hydrogenation to hydroxyl groups occurred, then hydrogenolysis took place, in line with the kinetics results. In addition, the bands corresponding to hydroxyl groups of B and C gradually decreased until they vanished as a result of hydrogenolysis. Finally, under *in-situ* conditions, the -CH_3 vibration peak of PX continuously increased with time. This result provided stronger evidence

that PX was generated. The *in-situ* infrared study once again confirmed the path of DMT conversion on $CuNa/SiO_2$, and the results are highly consistent with the kinetics behavior.

Based on the experimental data described above, we conducted a preliminary on-site test of an island using our method (Figure 5). A recent survey of beach sediment along the coastline of the Phuket Island showed that PET (mainly containing beverage bottles, plastic films, and microwave packaging) accounted for ca. 33.1% of the overall plastic sediment[23]. Our method achieved conversion of this sediment with 100% PX yield at 210°C on $CuNa/SiO_2$ in 6 h. Every ton of plastic sediment contained 331 kg of PET, and thus, 181 kg of PX and 105 kg of ethylene glycol (EG) could be obtained via this route under optimal conditions. The obtained PX and EG could be used as automobile fuel and antifreeze replenishment. As such, we demonstrated herein that $CuNa/SiO_2$ provides a viable option for processing waste PET accumulated on islands without a need of external hydrogen, transforming it into a high-value-added energy supply. This work could also help to solve the problem of waste resource conversion and reuse in the world today.

Conclusions

We report a H_2-free process for quantitatively converting PET plastic waste into PX and EG in methanol using low-cost $CuNa/SiO_2$ in a one-pot process. With the addition of NaCl during hydrothermal treatment, copper silicate with poor crystallinity, a small surface area, and a dense texture was formed. This material contained a high Cu^+/Cu^0 ratio of $Cu/Cu_2O{\cdot}SiO_2$ active sites, increasing the efficiency of the catalyst. The new system integrated PET degradation in methanol, methanol dehydrogenation, and DMT hydrodeoxygenation. We estimated that 331 kg of PET could be gathered in one ton of beach sediment, which would yield 181 kg of PX (gasoline components) and 105 kg of EG (automobile antifreeze) using the low-cost Cu-based catalyst in a one-pot process. The new process could be applied on islands with scarce resources and high accumulation degrees of ocean plastics. The products can be directly used for vehicle energy supply, benefiting the economy of the islands. The process is one-pot (allowing the entire process to be highly integrated), does not require an external hydrogen source, and uses low-cost hydrodeoxygenation catalysts, which provides a feasible method for converting waste plastics to high-value chemicals at a low cost.

References

1. PET polymer: chemical economics handbook. IHS Markit https://ihsmarkit.com/products/pet-polymer-chemical-economics-handbook.html. 2018.
2. Cornwall, W., The plastic eaters. *Science* 2021, *373* (6550), 36–39.
3. Meyer-Cifuentes, I. E.; Werner, J.; Jehmlich, N.; Will, S. E.; Neumann-Schaal, M.; Öztürk, B., Synergistic biodegradation of aromatic-aliphatic copolyester plastic by a marine microbial consortium. *Nature Communications* 2020, *11* (1), 5790.
4. Jambeck, J. R.; Geyer, R.; Wilcox, C.; Siegler, T. R.; Perryman, M.; Andrady, A.; Narayan, R.; Law, K. L., Plastic waste inputs from land into the ocean. *Science* 2015, *347* (6223), 768–771.
5. *Science* **2018**, *360* (6384), 28-29.
6. George, N.; Kurian, T., Recent Developments in the Chemical Recycling of Postconsumer Poly(ethylene terephthalate) Waste. *Industrial & Engineering Chemistry Research* **2014**, *53* (37), 14185–14198.
7. Thompson, R. C.; Olsen, Y.; Mitchell, R. P.; Davis, A.; Rowland, S. J.; John, A. W. G.; McGonigle, D.; Russell, A. E., Lost at Sea: Where Is All the Plastic? *Science* 2004, *304* (5672), 838–838.
8. Ügdüler, S.; Van Geem, K. M.; Denolf, R.; Roosen, M.; Mys, N.; Ragaert, K.; De Meester, S., Towards closed-loop recycling of multilayer and coloured PET plastic waste by alkaline hydrolysis. *Green Chemistry* 2020, *22* (16), 5376–5394.
9. Kang, M. J.; Yu, H. J.; Jegal, J.; Kim, H. S.; Cha, H. G., Depolymerization of PET into terephthalic acid in neutral media catalyzed by the ZSM-5 acidic catalyst. *Chemical Engineering Journal* 2020, *398*, 125655.
10. Mori, H.; Maeda, Y.; Kubota, S.; Yamaguchi, K.; Ito, O.; Maeda, T., Organosoluble Oligomer Obtained by Glycolysis of Poly(ethylene terephthalate) and Its Detailed Structural Characterization by MALDI-TOF Mass Spectrometry. *Polymer Journal* 2002, *34* (9), 687–691.
11. Mittal, A.; Soni, R. K.; Dutt, K.; Singh, S., Scanning electron microscopic study of hazardous waste flakes of polyethylene terephthalate (PET) by aminolysis and ammonolysis. *Journal of Hazardous Materials* 2010, *178* (1), 390–396.
12. Jing, Y.; Wang, Y.; Furukawa, S.; Xia, J.; Sun, C.; Hülsey, M. J.; Wang, H.; Guo, Y.; Liu, X.; Yan, N., Towards the Circular Economy: Converting Aromatic Plastic Waste Back to Arenes over a Ru/Nb2O5 Catalyst. *Angewandte Chemie International Edition* 2021, *60*

(10), 5527–5535.

13. Lu, S.; Jing, Y.; Feng, B.; Guo, Y.; Liu, X.; Wang, Y., H2-free Plastic Conversion: Converting PET back to BTX by Unlocking Hidden Hydrogen. *ChemSusChem n/a* (n/a).
14. Hongkailers, S.; Jing, Y.; Wang, Y.; Hinchiranan, N.; Yan, N., Recovery of Arenes from Polyethylene Terephthalate (PET) over a Co/TiO2 Catalyst. *ChemSusChem* 2021, *14* (19), 4330–4339.
15. Tang, H.; Li, N.; Li, G.; Wang, A.; Cong, Y.; Xu, G.; Wang, X.; Zhang, T., Synthesis of gasoline and jet fuel range cycloalkanes and aromatics from poly(ethylene terephthalate) waste. *Green Chemistry* 2019, *21* (10), 2709–2719.
16. Uekert, T.; Kuehnel, M. F.; Wakerley, D. W.; Reisner, E., Plastic waste as a feedstock for solar-driven H2 generation. *Energy & Environmental Science* 2018, *11* (10), 2853–2857.
17. Zhou, H.; Ren, Y.; Li, Z.; Xu, M.; Wang, Y.; Ge, R.; Kong, X.; Zheng, L.; Duan, H., Electrocatalytic upcycling of polyethylene terephthalate to commodity chemicals and H2 fuel. *Nature Communications* 2021, *12* (1), 4679.
18. Zhang, F.; Zeng, M.; Yappert, R. D.; Sun, J.; Lee, Y.-H.; LaPointe, A. M.; Peters, B.; Abu-Omar, M. M.; Scott, S. L., Polyethylene upcycling to long-chain alkylaromatics by tandem hydrogenolysis/aromatization. *Science* 2020, *370* (6515), 437–441.
19. Tennakoon, A.; Wu, X.; Paterson, A. L.; Patnaik, S.; Pei, Y.; LaPointe, A. M.; Ammal, S. C.; Hackler, R. A.; Heyden, A.; Slowing, I. I.; Coates, G. W.; Delferro, M.; Peters, B.; Huang, W.; Sadow, A. D.; Perras, F. A., Catalytic upcycling of high-density polyethylene via a processive mechanism. *Nature Catalysis* 2020, *3* (11), 893–901.
20. Li, B.; Li, L.; Sun, H.; Zhao, C., Selective Deoxygenation of Aqueous Furfural to 2-Methylfuran over $Cu^0/Cu_2O{\cdot}SiO_2$ Sites via a Copper Phyllosilicate Precursor without Extraneous Gas. *ACS Sustainable Chemistry & Engineering* 2018, *6* (9), 12096–12103.
21. Wu, L.; Li, B.; Zhao, C., Direct Synthesis of Hydrogen and Dimethoxylmethane from Methanol on Copper/Silica Catalysts with Optimal Cu^+/Cu^0 Sites. *ChemCatChem* 2018, *10* (5), 1140–1147.
22. Wu, L.; Li, L.; Li, B.; Zhao, C., Selective conversion of coconut oil to fatty alcohols in methanol over a hydrothermally prepared Cu/SiO_2 catalyst without extraneous hydrogen. *Chemical Communications* **2017**, *53* (45), 6152–6155.
23. Akkajit, P.; Tipmanee, D.; Cherdsukjai, P.; Suteerasak, T.; Thongnonghin, S., Occurrence and distribution of microplastics in beach sediments along Phuket coastline. *Marine Pollution Bulletin* 2021, *169*, 112496.

Figures

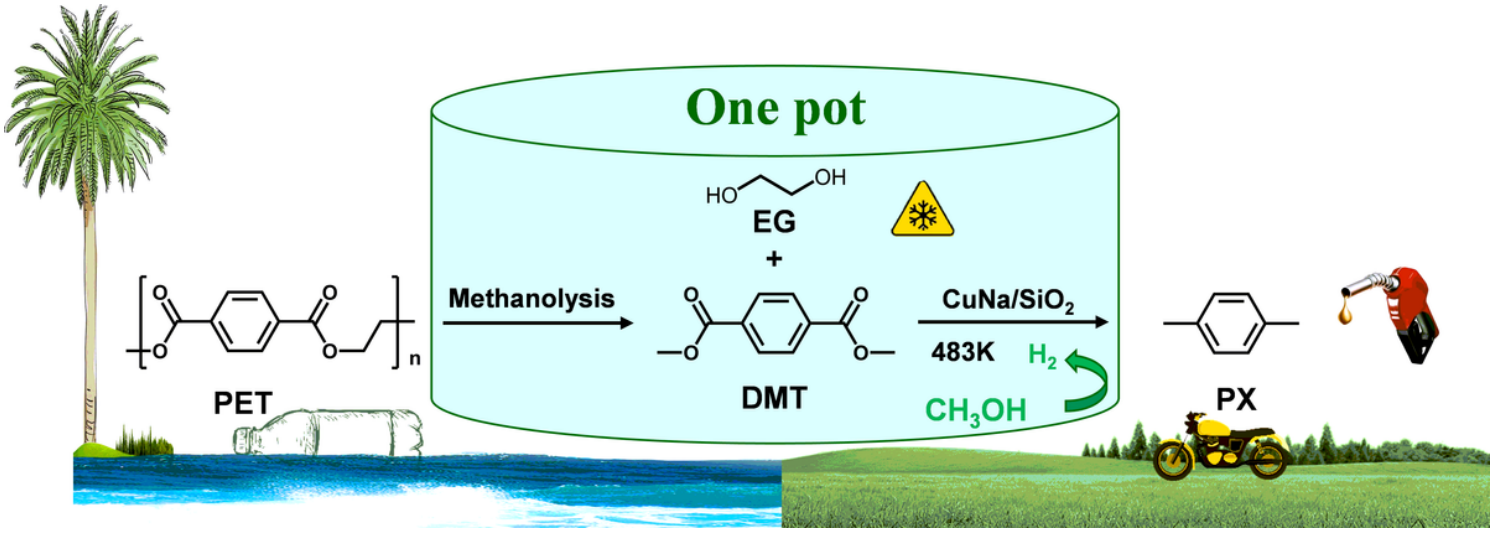

Figure 1

Strategy for the depolymerization and conversion of polyethylene terephthalate (PET) wastes.

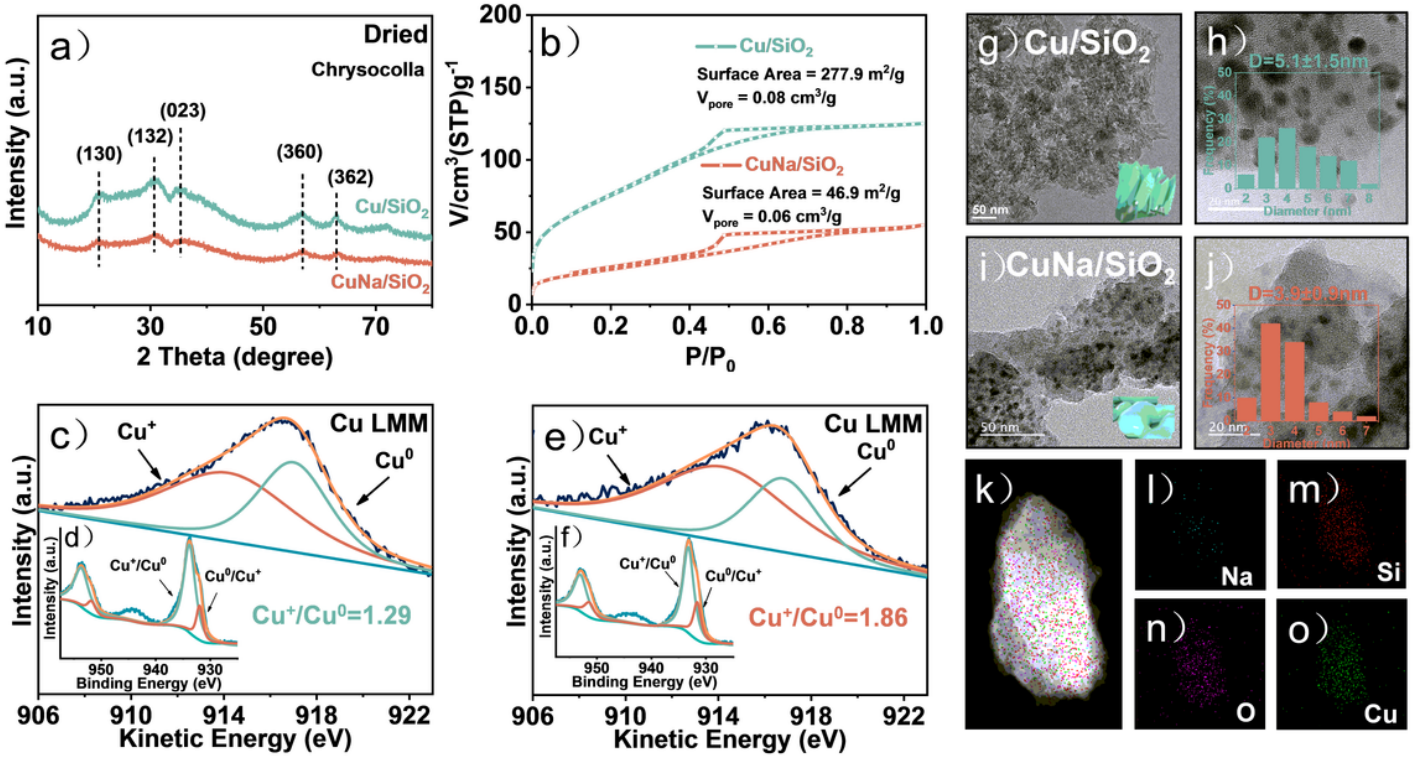

Figure 2

(a) X-ray diffraction (XRD) patterns of Cu/SiO2 (dried) and CuNa/SiO2 (dried). (b) N2 adsorption–desorption of Cu/SiO2 (dried) and CuNa/SiO2 (dried). X-ray photoelectron spectroscopy (XPS) Cu 2p spectra of (d) Cu/SiO2 (reduced) and (f) CuNa/SiO2 (reduced). Cu LMM X-ray induced Auger electron spectroscopy (XAES) spectra of (c) Cu/SiO2 (reduced) and (e) CuNa/SiO2 (reduced). (g) Transmission electron microscopy (TEM) images of Cu/SiO2 (dried), (h) Cu/SiO2 (reduced) at a higher magnification, (i) CuNa/SiO2 (dried), (j) and CuNa/SiO2 (reduced) at higher magnification. (k) Transmission electron spectroscopy–energy dispersive X-ray spectroscopy (TEM-EDS) mappings of the elements in CuNa/SiO2: (l) Na, (m) Si, (n) O, and (o) Cu.

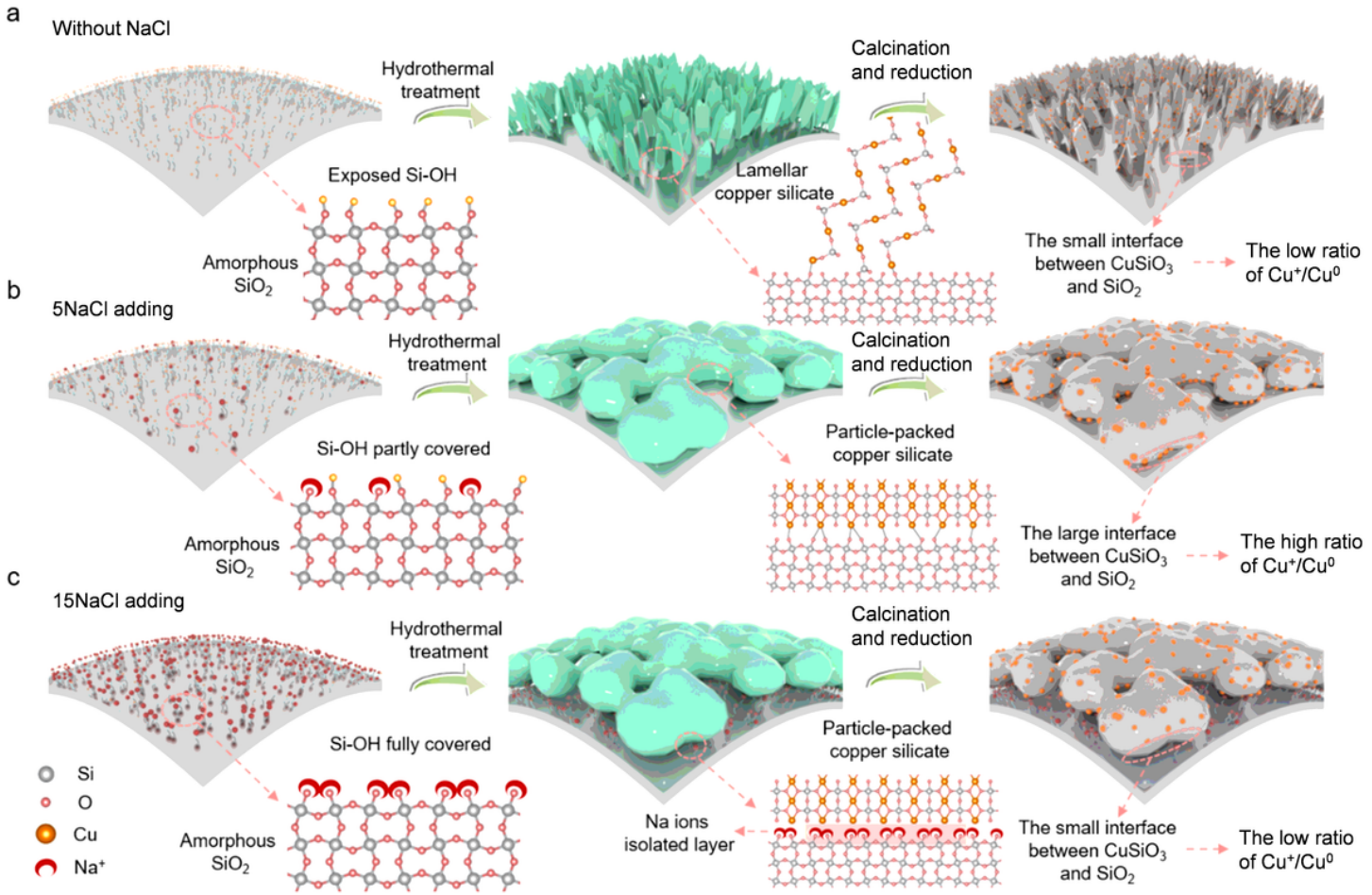

Figure 3

Three copper silicate formation processes with different amounts of introduced NaCl.

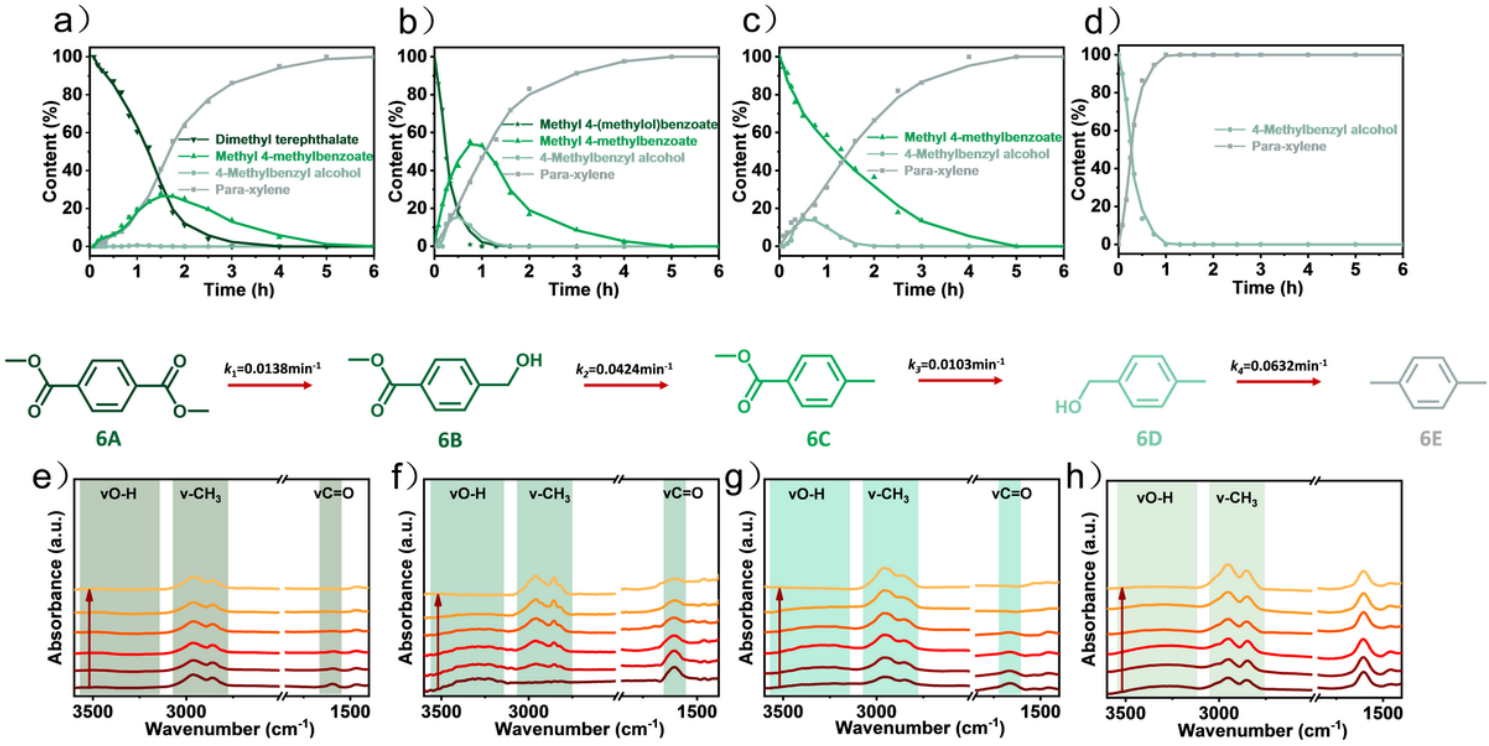

Figure 4

Product distribution–reaction time curves for the catalytic conversion of: (a) dimethyl terephthalate, (b) methyl 4-(methylol)benzoate, (c) methyl 4-methylbenzoate, and (d) 4-methylbenzyl alcohol on CuNa/SiO2. Reaction conditions: PET, 0.12 g; CuNa/SiO2 catalyst, 0.1 g; methanol, 30 mL; 210 °C; 6 h. Time-resolved in-situ transmitted Fourier-transform infrared spectroscopy difference spectra of (e) dimethyl terephthalate, (f) methyl 4-(methylol)benzoate, (g) methyl 4-methylbenzoate, and (h) 4-methylbenzyl alcohol at 120 °C from 10 to 60 min on CuNa/SiO2.

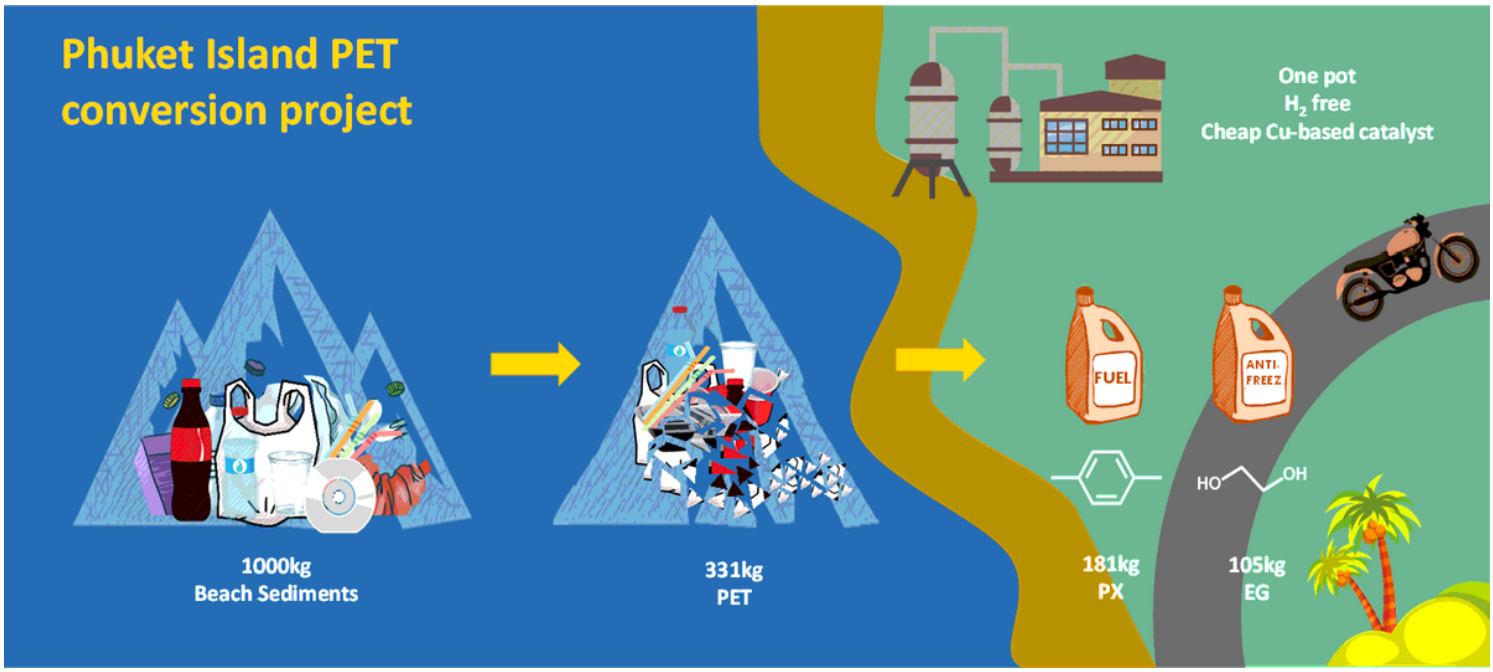

Figure 5

Results of the application of our new PET conversion catalytic route on sediment from the Phuket Island.

Supplementary Files

This is a list of supplementary files associated with this preprint. Click to download.

- SIConvertingwastePETplasticsintoautomobilefuelandantifreezecomponents.docx